Available online at www.sciencedirect.com
ScienceDirect
International Journal of Solids and Structures 44 (2007) 6999–7020
INTERNATIONAL JOURNAL OF SOLIDS AND STRUCTURES
www.elsevier.com/locate/ijsolstr

Influence of fibre orientation and stacking sequence on petalling of glass/polyester composite cylindrical shells under axial compression

S. Solaimurugan, R. Velmurugan *

Composites Technology Centre, Indian Institute of Technology Madras, Chennai 600 036, India

Received 22 December 2006; received in revised form 21 March 2007
Available online 30 March 2007

Abstract

The energy absorbing capability of FRP composite cylindrical tubes used as energy absorbers, by destroying itself progressively, depends on the way in which the tube material is crushed i.e., trend of petalling. This paper investigates the influence of fibre orientation and stacking sequence on the petal formation and specific energy absorption (SEA) of four and six-ply, 0°/90° glass/polyester composite cylindrical shells under axial compression. Number of petals formed and the trend of petalling are changed with proportion of axial (0°) and circumferential (90°) fibre content and stacking sequence in the tubes. In the tubes undergo petalling, presence of axial fibres close to inner surface and the proper proportion of circumferential fibres close to outer surface of the tube wall lead to higher energy dissipation. The axial fibres placed nearer to outer surface leads to more number of petal formation, leading to a stable crushing mechanism. The contribution of mode I strain energy release rate (G_{Ic}) to the energy dissipation in the form of circumferential delamination is also studied with double cantilever beam (DCB) tests. Analytical model which considers petalling is developed, and used to predict the mean crush load and SEA of cylindrical composite shells under axial compression. Results from the analytical model agree well with experimental results and are presented.

Keywords: Petalling; Fracture toughness; Progressive crushing; Fibre orientation; Stacking sequence; Polymer-matrix composites

1. Introduction

Advances in automotive and aircraft sectors lead to production of luxurious and very high speed vehicles. Eventhough lot of comfortable facilities have come, passenger's safety is the prominent requirement. The amount of energy that a vehicle absorbs during collision is a matter of concern to ensure safer and more reliable vehicles. So, the need of better vehicle crashworthiness has directed the researcher's attention towards the usage of FRP composites as collapsible absorbers of crash energy (Mamalis et al., 2004), since the composite structural members dissipate huge amount of energy during collision and improves the vehicle crashworthiness.

* Corresponding author. Tel.: +91 44 22574017; fax: +91 44 22570039.
E-mail address: rvel@iitm.ac.in (R. Velmurugan).

0020-7683/$ - see front matter © 2007 Elsevier Ltd. All rights reserved.
doi:10.1016/j.ijsolstr.2007.03.025

Nomenclature

WRM	woven roving glass fibre mat
UD	unidirectional glass fibre mat
0°	fibre orientation along the tube axis and along the length of planar specimen
90°	fibre orientation along the circumferential direction of tube and along the width of planar specimen
SEA	specific energy absorption (J/kg)
G_{Ic}	mode I interlaminar fracture toughness (kJ/m^2)
h	stroke length for axial crushing of cylindrical shell
U_d	energy required for circumferential delamination (J)
U_a	energy required for petal formation (axial cracks) (J)
U_b	energy required for bending of petals (J)
U_f	energy dissipated due to friction between crushing platen and petals (J)
W_e	external work done by applied force P (J)
K_I	mode I stress intensity factor
E	Young's modulus (Pa)
n	number of petals
σ	circumferential stress
σ_u	fracture strength in uni-axial tension (MPa)
σ_b	flexural strength (MPa)
σ_s	interlaminar short beam shear strength (MPa)
θ	bending angle of petals
μ	co-efficient of friction between petal and crushing platen
D, r	diameter and radius of cylindrical shell (mm)
H, t	height and thickness of cylindrical shell (mm)
W	externally applied load for DCB test (N)
δ	load point deflection of DCB specimen (mm)
a	instantaneous crack length in DCB test (mm)
Δ	effective delamination extension correction factor for DCB specimen
C	compliance of DCB specimen ($C = \delta/W$)

Nowadays, the automotive industries are exploring to adopt fibre reinforced polyester-matrix composites into automobile bodies, because, they offer the stiffness of conventional metals at lower weight. FRP composite bumper beam is one of the main components of car that protect passengers from front and rear collision (Hosseinzadeh et al., 2005). Thin walled composite cylindrical tubes are common structural components that can be used for a wide variety of applications including drive shafts, chassis of automobiles, trusses for space vehicles and oil pipelines etc, and are used as energy absorbers (Farley, 1991; Mamalis et al., 1997; Hull, 1991).

The energy absorbing capability of axially collapsed thin walled composite shells depends on the fracture behavior of the shell. The shell which collapses in a stable, progressive and controlled manner can dissipate large amount of energy (Mamalis et al., 1997; Hull, 1991; Bisagni et al., 2005; Mamalis et al., 2006). Progressive deformation and stable collapse significantly reduce the forces experienced by the passengers in the event of sudden collision (Mamalis et al., 2004). It has been observed that composite cylindrical tubes with D/t ratios greater than 66 fail catastrophically where as tubes with D/t ratios in the range 4–66 crush progressively (Hamada and Ramakrishna, 1995). Though the SEA increases with decreasing D, SEA mainly depends on the absolute value of t, rather than the D/t ratio. For a given value of D, SEA increases with increasing t up to certain value above which it decreases. Highest energy absorption capability has been displayed by tubes of thickness in the range of 2–3 mm (Hamada and Ramakrishna, 1995). Tao et al. (2005) have analyzed the energy absorption capability of 3D braided composite tubes. They have reported that the total energy absorption increases with increase in thickness of tube wall, while SEA increases with increase in t up to 3 mm

beyond which SEA reaches the plateau state. In this work, we have selected two sets of tubular specimens with D/t ratios around 15 and 25, each set have specimens of different proportions of axial and circumferential fibres and stacking sequence.

Hull (1991) has experimentally studied the progressive crushing of fibre reinforced composite tubes. He has observed that the splaying mode crush zone contains features such as debris wedge splitting the tube wall into fronds, longitudinal cracks, frond splitting into thin beams and fractured fibres. He expected that the following five groups of forces may act in the crush zone of axially crushed cylindrical shell, and are

(i) Compressive forces acting at the platen on the fronds and the debris wedge.
(ii) Friction at the platen owing to the sliding of the splayed fronds across the platen surface as crushing proceeds.
(iii) Friction between the debris wedge and the fronds.
(iv) Friction between adjacent laminae in the fronds as they bend through different radii of curvature.
(v) Hoop constraints resulting from crack opening along the centre of the tube wall.

The energy absorbed from the first force term is dissipated through all the remaining four force terms.

Researches are going on to improve the energy absorbing capability of composite cylindrical shells under axial compression. Gupta et al. (1997) and Reddy and Wall (1988) have analyzed the axially crushing foam filled composite and metallic cylindrical tubes, respectively, and observed the improved energy absorption comparing to hollow tubes. Failure by petalling is a controlled energy absorbing mechanism of thin walled composite cylindrical shells.

Petalling failure in plates has been analyzed by Landkof and Goldsmith (1985), Wierzbicki (1999) and Atkins et al. (1998), however, detailed data that related to petalling of composite cylindrical shells are not available. Alexander (1960) has presented a first theoretical model for the analysis of plastic collapse of a cylindrical metallic shell under axial load. Atkins (1987) has developed a model to predict the number of axial cracks which propagate in experiments on the splitting of axially crushed ductile metal tubes when the ends are flared out. The predictions of this model are well matched with experimental results reported by Reddy and Reid (1986). Similarly many models, describing the energy absorbing capacity of cylindrical metallic tubes (Alexander, 1960; Gupta and Abbas, 2000) and composite tubes (Tao et al., 2005; Gupta et al., 1997; Quek et al., 2001; Velmurugan et al., 2004; Farley and Jones, 1992) have been developed. In our earlier work (Solaimurugan and Velmurugan, 2007), we have studied the effect of stitching on specific energy absorption, SEA of progressively crushing composite cylindrical shells under axial compression.

In this present work, the influence of fibre orientation and stacking sequence on the petal formation and specific energy absorption, SEA of four and six-ply glass/polyester composite cylindrical shells under axial compression are studied experimentally and analytically. Energy dissipation through axial crack formation or petalling and petal bending is analyzed in this work by varying the proportion of axial, circumferential fibres and stacking sequence. The improvement of energy dissipation through circumferential delamination is also analyzed for various fibre orientations in the mid-plane interface of tube wall. The present work is carried out in quasi-static condition, and it is valid only when the tube deforms through petal formation which is one of the different failure modes; while the microfragmentation and splaying are other failure modes.

2. Fabrication and testing of specimens

Woven roving (WRM) glass fibre mats of density 610 g/m^2, unidirectional (UD) glass fibre mats of density 750 g/m^2 and isophthalic polyester resin were used for fabrication of planar and cylindrical specimens.

2.1. Planar specimens for mechanical properties

Series of planar laminates with two and three-ply of dimension 300 mm × 300 mm were fabricated with WRM, UD glass fibre mats and polyester resin. In order to study the mechanical properties of material splaying inside and outside of the four and six-ply tubes during crushing, two-ply (WRM/90, WRM/0) and three-ply (WRM/90/90, WRM/90/0, WRM/0/90, WRM/0/0) laminates, respectively, were prepared. The nominal

thickness of two and three-ply laminates were approximately 1.1 and 2 mm, respectively. The fibres oriented along the length of specimen are called as 0° fibres, while along the specimen width being 90° fibres. The WRM was aligned such that fibres were oriented along the length and width of specimens. Specimens were prepared with fibre weight fraction (W_f), of around 0.65, and post cured at 60 °C for 4 h.

Tensile, flexural and short beam shear test specimens were cut from each type of laminates. Dimensions of test specimens and their corresponding standards for the above tests are given in Table 1. The ultimate uniaxial tensile strength was obtained from tensile test. Flexural strength and interlaminar shear strength were obtained from flexural and short beam shear tests, respectively. The flexural and short beam shear tests were performed by 3-point bending. At least three test samples for each specimen were performed. All the tests were carried out in the Instron UTM of model 4301 under quasi-static loading with a crosshead speed of 2 mm/min.

2.2. Double cantilever beam (DCB) test specimens

Double cantilever beam (DCB) test specimens having dimensions as per standard ASTM D5528-01were cut from various planar laminates having 0°/0°, 0°/90°, 90°/90° mid-plane interface, to determine the mode I interlaminar fracture toughness, G_{Ic}. A non-adhesive Teflon film was inserted in the mid-plane of the laminate during fabrication to form an initiation site for the delamination. The loading hinges were mounted at the end of DCB specimen arms. DCB test was carried out in the Instron UTM of model 4301. The predelaminated end of the DCB specimen was opened by quasi-static loading in the controlled crosshead speed of 2 mm/min. The curves between load and crack opening displacement were drawn and the locations of instantaneous delamination front were marked at intervals of delamination growth. Five specimen samples for each DCB test were performed.

2.3. Cylindrical specimens

The cylindrical tubular specimens of four and six-ply were prepared from WRM, UD glass fibre mats and polyester resin by hand lay-up with various stacking sequence and fibre orientation. Cylindrical preforms have WRM mats as outer and inner most layer of the tube wall, and the UD mats are placed in between, [WRM/$(UD)_m$/WRM]; m being 2 and 4 for four and six-ply tubes. The stacking sequence from outer surface to inner surface of tube is represented from left to right. The fibres oriented along the axis of tube are termed as 0° fibres, while along the circumferential direction being 90° fibres. Woven roving mat, WRM was aligned such that fibres were being oriented along the axial and hoop directions. The four and six-ply tubes made with various proportions of 0° and 90° fibres, and the stacking sequence were classified into C and D series, respectively. In the C1 and D1 tubes, 50% fibres of WRM and all the 100% fibres of UD mat are oriented along the circumferential direction, and the remaining fibres along the axial direction. Similarly the C4 and D7 tubes have 50% fibres of WRM and all the 100% fibres of UD mat oriented along the axial direction, and the remaining fibres along the circumferential direction. The C2, C3, D2, D3 and D4 tubes have equal amount of fibres along the axial and circumferential directions with various stacking sequence. The D5 and D6 tubes have 50% fibres of WRM and 75% fibres of UD along the axial direction, and the remaining fibres along the circumferential direction.

The preforms were separately wound on wooden mandrel of 60 mm diameter with longitudinal overlap of around 10 mm. The cylindrical fabrics were impregnated with isophthalic polyester resin. The tubes were post cured at 60 °C for 4 h and cut for the height approximately equal to 2.5 times the diameter.

Table 1
Test standards and dimensions of planar specimens

Sl. No.	Test	Standard	Specimen dimensions	
			Length (mm)	Width (mm)
1	Tensile test	ASTM D3039/ISO 3268-75	230	25
2	Flexural test	ASTM D790-00/ISO 178-75	80	10
3	Short beam shear test	ASTM D2344-00	Six times the thickness	10

It has been reported that the global buckling and catastrophic failure of axially crushed composite cylindrical tubes can be avoided by maintaining the D/t ratio between 15 and 40 (Gupta et al., 1997). Here, four and six-ply tubes have same inner diameter but different thicknesses and hence D/t ratios of around 15 and 25 were obtained, respectively. One end of the tube was chamfered with an external angle of 30°, which provided the triggering mechanism for progressive crushing. Chamfering also avoided catastrophic brittle failure, because average progressive crushing stress was lower than brittle failure stress (Farley and Jones, 1992; Daniel et al., 2000). Since the quasi-static tube crush is the representative test which provides the correct overall trend that is experienced by a composite member during a crash (Quek et al., 2001), tubular specimens were subjected to axial compression in the UTM with a crosshead speed of 2 mm/min.

3. Results and discussion

All the planar and tubular specimens were tested under quasi-static condition with a crosshead speed of 2 mm/min. All the laminates are the kind of cross ply laminates i.e., fibres are oriented along the warp and weft directions only in case of planar specimens, and along axial and hoop directions only in case of cylindrical specimens.

3.1. Mechanical properties

The planar specimens were cut from the laminate, and the experiments were performed as per standards reported in Table 1. Specimens were tested for tensile, flexural and short beam shear strengths, and the values are reported in Table 2. It is observed that tensile, flexural and short beam shear strengths are increased with increase in proportion of fibres oriented along the specimen length.

3.2. Mode I interlaminar fracture toughness

The DCB test as per ASTM D5528-01 was carried out and the mode I interlaminar fracture toughness, G_{Ic} was determined. The DCB test setup with specimen being tested is shown in Fig. 1. The modified beam theory expression (ASTM D5528-01) used for calculating the strain energy release rate of double cantilever beam is

$$G_{Ic} = \frac{3W\delta}{2b(a + |\Delta|)} \tag{1}$$

where W is applied load, δ is load point deflection, b is specimen width, a is instantaneous crack length and Δ is effective delamination extension correction factor for the rotation of DCB arms at delamination front. Δ is determined experimentally by generating a least square plot of the cube root of compliance, $C^{1/3}$, as a function of delamination length. The compliance C is the ratio of the load point displacement to the applied load, δ/W.

The delamination resistance curves (R-curves) are drawn between crack length and mode I interlaminar fracture toughness (G_{Ic}), and one of them is shown in Fig. 2. The G_{Ic} values corresponding to the points of

Table 2
Mechanical properties of planar specimens

Specimen ID	Layer orientation	Tensile strength, σ_u (MPa)	Short beam shear strength, σ_s (MPa)	Flexural strength, σ_b (MPa)
Two-ply planar specimens				
A1	WRM/90	84.3 ± 2.4	26.8 ± 3	76.95 ± 5.6
A2	WRM/0	320.5 ± 25	48.4 ± 2	937.9 ± 60
Three-ply planar specimens				
B1	WRM/90/90	68.47 ± 3.1	25.53 ± 6.1	30.37 ± 2.6
B2	WRM/0/90	264.43 ± 17.3	29.98 ± 1.89	295 ± 19.6
B3	WRM/90/0	264.43 ± 17.3	33.5 ± 3	474.26 ± 24
B4	WRM/0/0	400 ± 15	42.01 ± 0.41	593.45 ± 54.7

0°-fibre orientation along the length of specimen; 90°-fibre orientation along the specimen width.

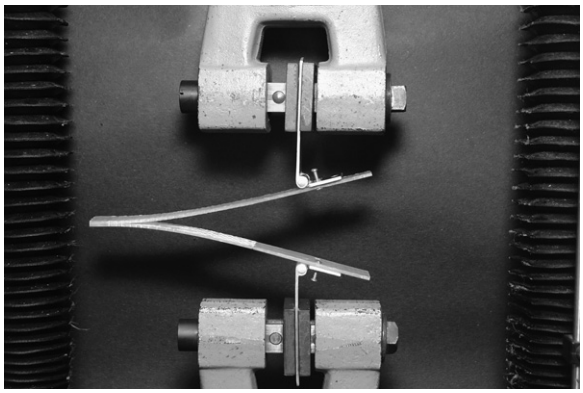

Fig. 1. DCB test setup in UTM.

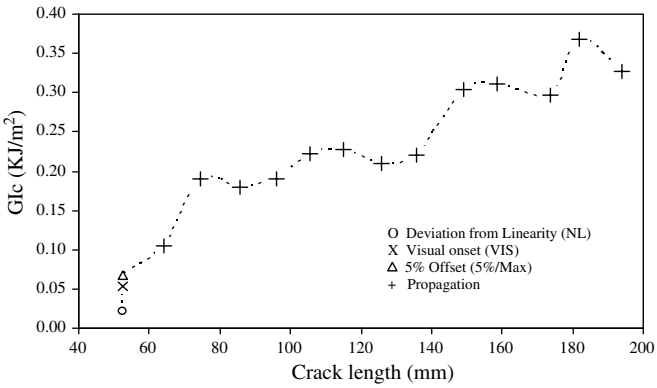

Fig. 2. Resistance curve (*R*-curve) between critical Mode I strain energy release rate and crack length for the DCB specimen.

Deviation from Linearity (NL), Visual Observation (VIS) and 5% Offset/Maximum load (5%/Max) are also shown in the *R*-curve. The G_{Ic} value corresponding to first crack initiation is determined from film insert. The G_{Ic} values are taken from the plateau region (Velmurugan and Solaimurugan, 2007; Shah Khan and Mouritz, 1996) of the *R*-curves and thus represent the steady state delamination fracture toughness.

It is observed from Table 3 that G_{Ic} of planar specimens not only depends on the property of resin material between adjacent layers, but also depends on the fibre orientation in the layers adjacent to the fracture plane. It is observed that 0/90 interface has higher G_{Ic} comparing to 0/0 and 90/90 interfaces.

3.3. Progressive crushing of cylindrical shells

Tubular samples of length around 160 mm were cut, and the one end was chamfered while the other end was flat as shown in Fig. 3. Three samples of each tube were tested. Each sample was crushed for the crush distance of about 120 mm in the UTM between hardened steel flat platens. Tested specimens of four and six-ply tubes are shown in Figs. 4 and 5, respectively. Crushing starts with chamfered portion of the samples. Initially the chamfered portion of the tube is crushed into flat and then local buckling occurs due to axial compression load followed by circumferential delamination. Further crushing on the circumferentially delaminated layers leads to severe circumferential strain causing axial or longitudinal cracks. This results into formation of number of symmetric petals. Crushing then continues with circumferential delamination and axial cracking of the outermost layers.

The load–load point displacement curves of four and six-ply tubes are plotted, and are shown in Figs. 6 and 7. The first peak load corresponds to the complete crush of the chamfered zone of specimen. Once the first

Table 3
Mode I interlaminar fracture toughness

Fracture plane interface	Material	Lay-up sequence	Interlaminar fracture toughness G_{Ic} (kJ/m^2)
0/90	Glass (WRM-610 g/m^2, UD-750 g/m^2)/ polyester	WRM/90/0/90/0/ WRM	0.524 ± 0.006
90/90	Glass (WRM-610 g/m^2, UD-750 g/m^2)/ polyester	WRM/0/90/90/0/ WRM	0.481 ± 0.015
0/0	Glass (WRM-610 g/m^2, UD-750 g/m^2)/ polyester	WRM/0/0/0/0/WRM	0.358 ± 0.075

peak load is attained, the shell is crushed progressively. During progressive crushing, the lip of the tube experiences large strain, and half of the thickness of tube wall flares inwards and the remaining half of the thickness flares outwards into fronds. Figs. 4 and 5 show that the crush zone has fronds of material splaying outside the shell whereas the material splaying inside does not form fronds, and just bends inside the tube. Brittleness of the tube material attributes the circumferential and axial cracks to propagate through successive cycles towards other end of the tube and thus loads oscillate around mean crush load.

It has been assumed (Alexander, 1960) in axial crushing of metallic tubes that one fold is formed at a time and further assumed that a given fold element goes through the entire crushing process before its neighbor begins to deform. After the element is crushed, the tube returns to its ultimate compressive capacity at the end of each cycle; a characteristic which is not observed experimentally (Alexander, 1960). But here, the debris formed during crushing are entrapped within the circumferentially delaminated zone between the materials flared inwards and outwards. The debris acts as a wedge, and causes the circumferential delamination

Fig. 3. Cylindrical shell with chamfered end.

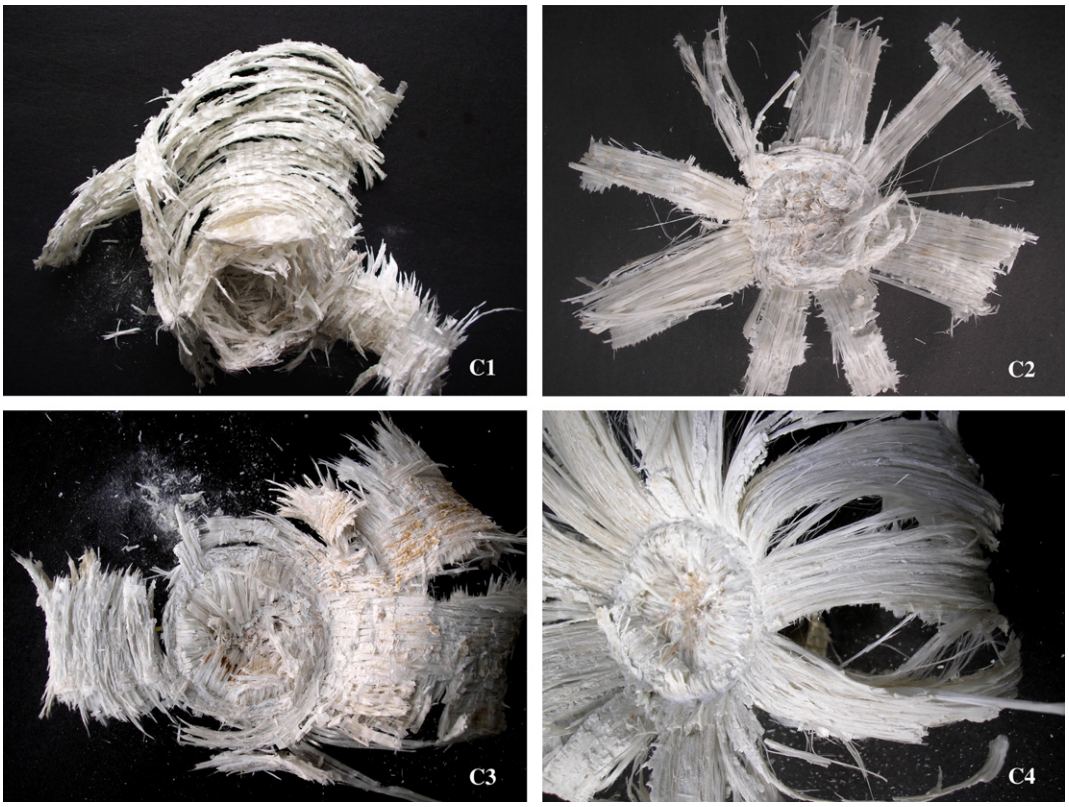

Fig. 4. Tested four-ply tubular specimens. C1 [WRM/$(90)_2$/WRM], C2 [WRM/0/90/WRM], C3 [WRM/90/0/WRM], C4 [WRM/$(0)_2$/WRM].

propagation in advance to the root of petal i.e., the bottom hinge point of petal. The SEM picture of crush zone is illustrated in Fig. 8a. In Fig. 8b, the SEM picture of the crush zone, the delamination crack front is observed 10 mm away in the propagation side from the root of petal formed in the previous cycle, before the petal has completely broken at its root due to compressive load by crushing platen.

As the initial slope of the load–displacement curve depends on the chamfer angle, mean crush load is calculated in the steady state crush zone. Specific energy absorption, SEA is calculated as the area under the mean crush load of load–displacement curve per unit mass of tube material crushed. None of the specimen shows failure along the overlap zone of the tube during progressive crushing.

3.4. Petalling

The SEA depends on the trend inwhich the material is crushed i.e., trend of petalling process. The petals formed through well defined and stable axial cracking lead to higher SEA. It is observed that the energy dissipated through circumferential delamination, axial crack or petal formation, and petal bending depends on the fibre orientation and stacking sequence. The number of petals observed in all the four and six-layered tubes is reported in Table 4.

3.4.1. Four-ply tubes ($D/t = 25$)

In the case of four-layered C1 and C3 specimens, the outermost WRM layer and its adjacent circumferential layer flare outwards, while the remaining layers flare inwards. The presence of hoop fibres close to the outer surface does not allow several axial cracks. In the WRM/$(90)_2$/WRM (C1) tubes, only two axial cracks are formed which lead to one small petal and another very big petal in the form of bellows that covers around 300° of the tube circumference as in Fig. 4, whereas in the C3 specimen three petals of almost equal width are

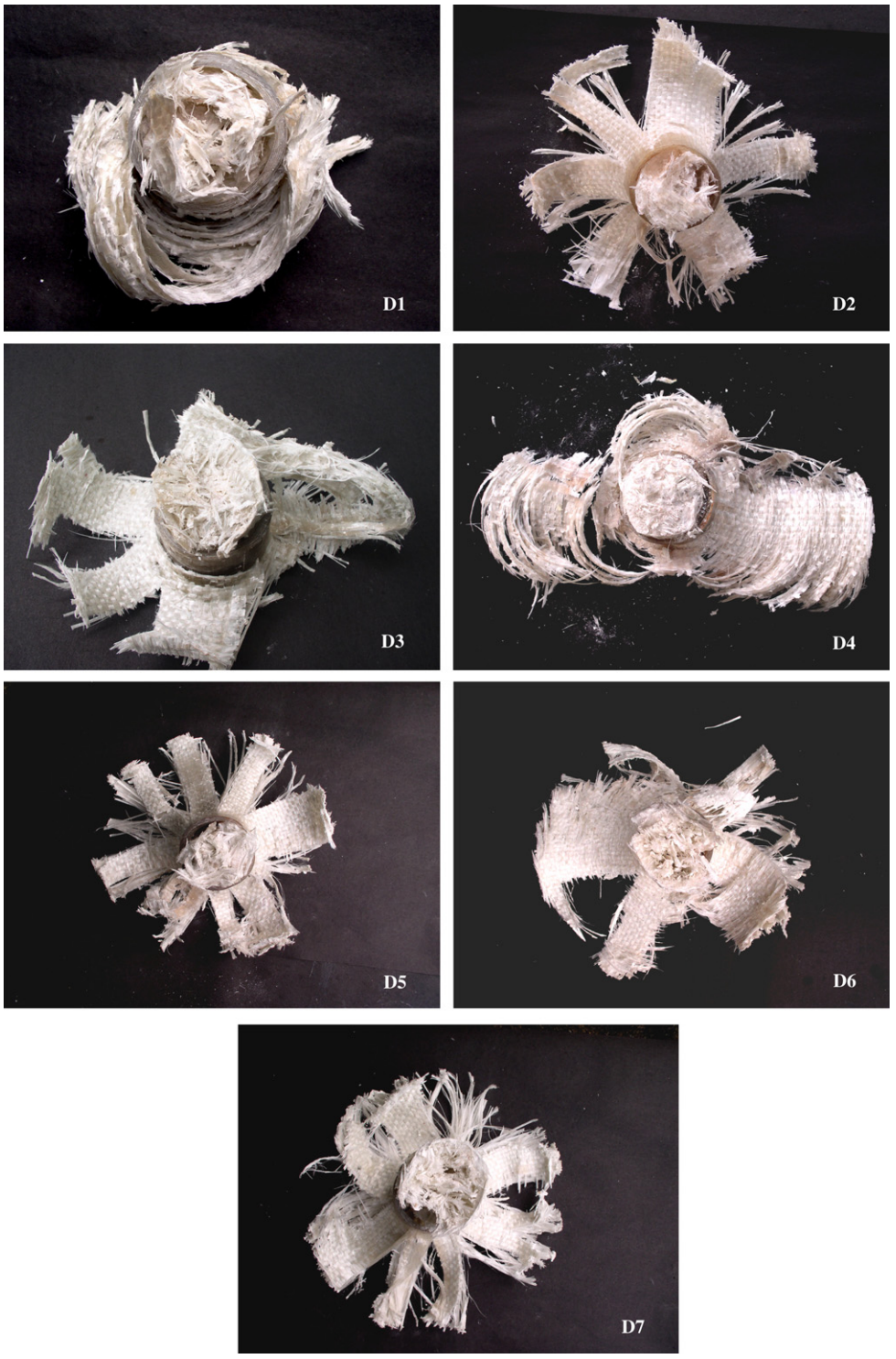

Fig. 5. Tested six-ply tubular specimens. D1 [WRM/$(90)_4$/WRM], D2 [WRM/$(0)_2$/$(90)_2$/WRM], D3 [WRM/$(90/0)_2$/WRM], D4 [WRM/$(90)_2$/$(0)_2$/WRM], D5 [WRM/$(0)_3$/90/WRM], D6 [WRM/90/$(0)_3$/WRM], D7 [WRM/$(0)_4$/WRM].

formed. Whenever the two adjacent UD layers in a laminate have same fibre orientation, they act as single layer, and the interlaminar delamination cannot merely separate these two layers. Instead, these two adjacent

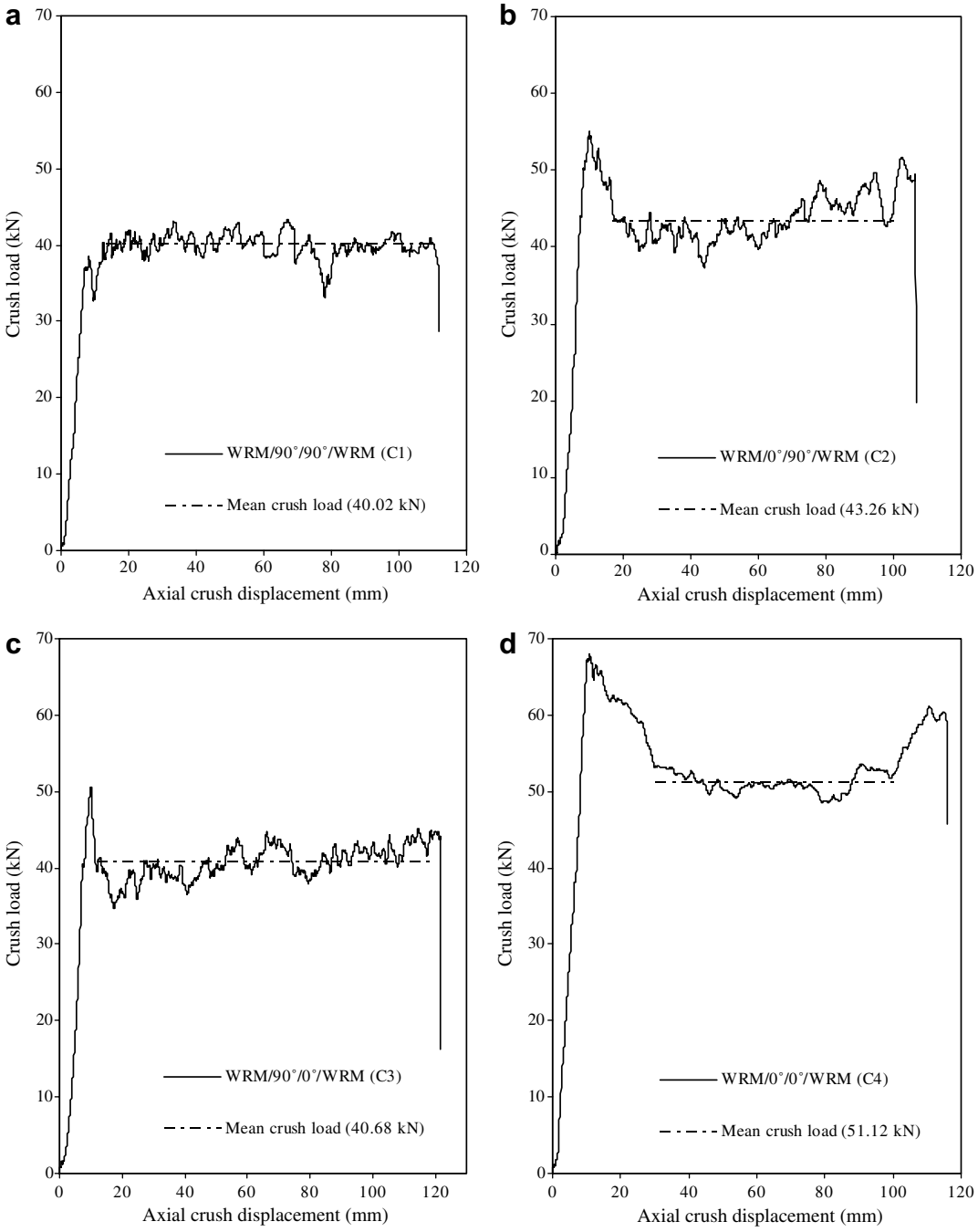

Fig. 6. Crush load–axial crush displacement plots of four-ply tubes ($D/t = 25$), (a) WRM/$(90)_2$/WRM (C1), (b) WRM/0/90/WRM (C2), (c) WRM/90/0/WRM (C3), (d) WRM/$(0)_2$/WRM (C4).

layers share their fibres during delamination. So, higher resistance to axial crack is offered in WRM/$(90)_2$/WRM tubes than in WRM/90/0/WRM tubes.

When the four-layered C2 and C4 specimens are crushed, the outermost WRM layer and its adjacent longitudinal layer flare outwards into petals and the remaining layers flare inwards. In these C2 and C4 specimens, well defined axial cracks are observed due to the presence of axial fibres nearer to the outer surface of the tube (Fig. 4). The C1 tubes have SEA of 35623 J/kg, which is the lowest SEA of C-series tubes, whereas

the fibre orientation in C4 tubes leads to the maximum SEA, which is 25% higher than that of C1 tubes. The C2 and C3 tubes have 2.7% and 9% higher SEA comparing to C1 tubes. The SEA variation of tubes ($D/t = 25$) with the proportion of axial fibre content is shown in Fig. 9. The differences observed in the SEA between samples cut from the same tube are reported as standard deviation in Table 4.

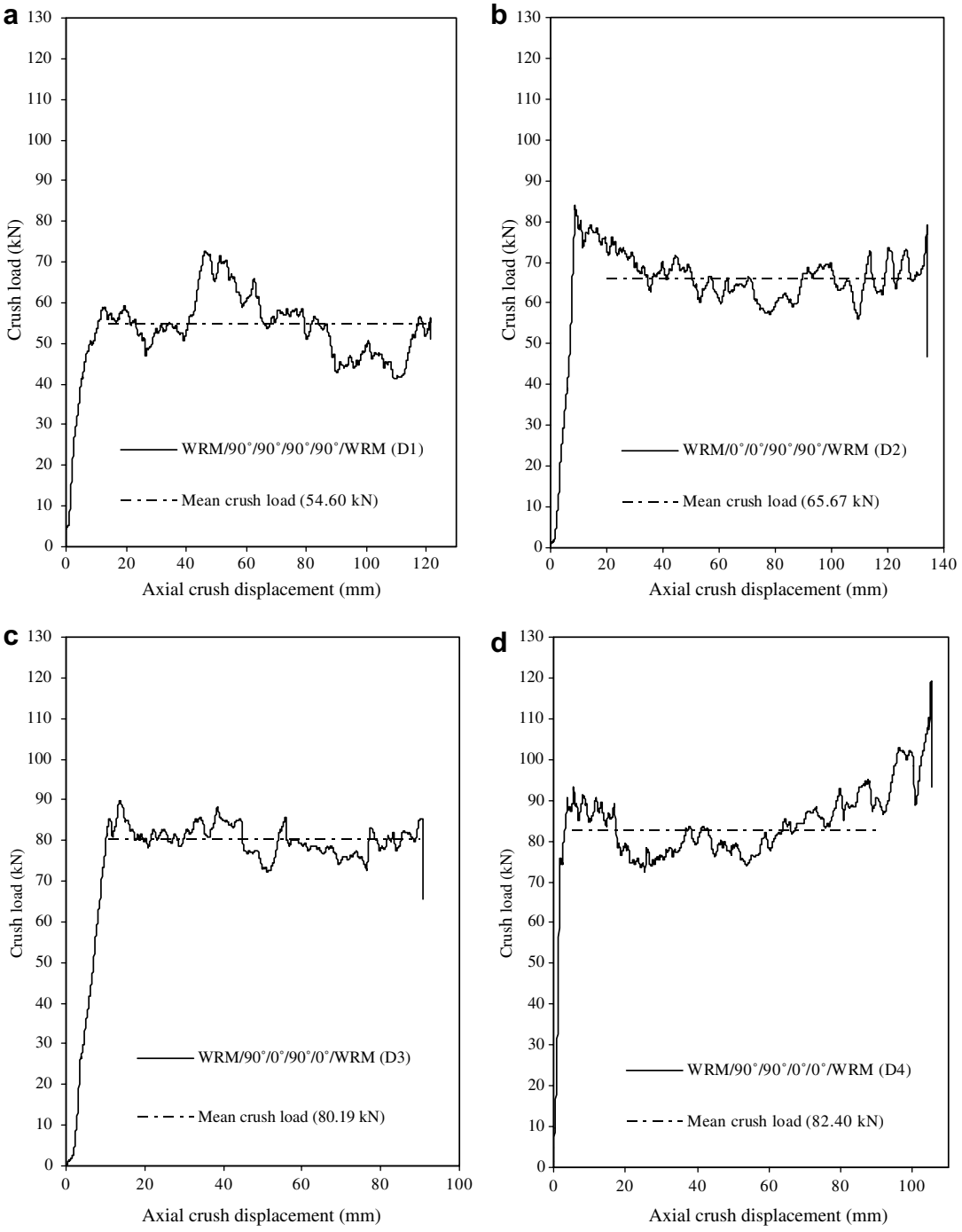

Fig. 7. Crush load–axial crush displacement plots of six-ply tubes ($D/t = 15$), (a) WRM/$(90)_4$/WRM (D1), (b) WRM/$(0)_2$/$(90)_2$/WRM (D2), (c) WRM/$(90/0)_2$/WRM (D3), (d) WRM/$(90)_2$/$(0)_2$/WRM (D4), (e) WRM/$(0)_3$/90/WRM (D5), (f) WRM/90/$(0)_3$/WRM (D6), (g) WRM/$(0)_4$/WRM (D7).

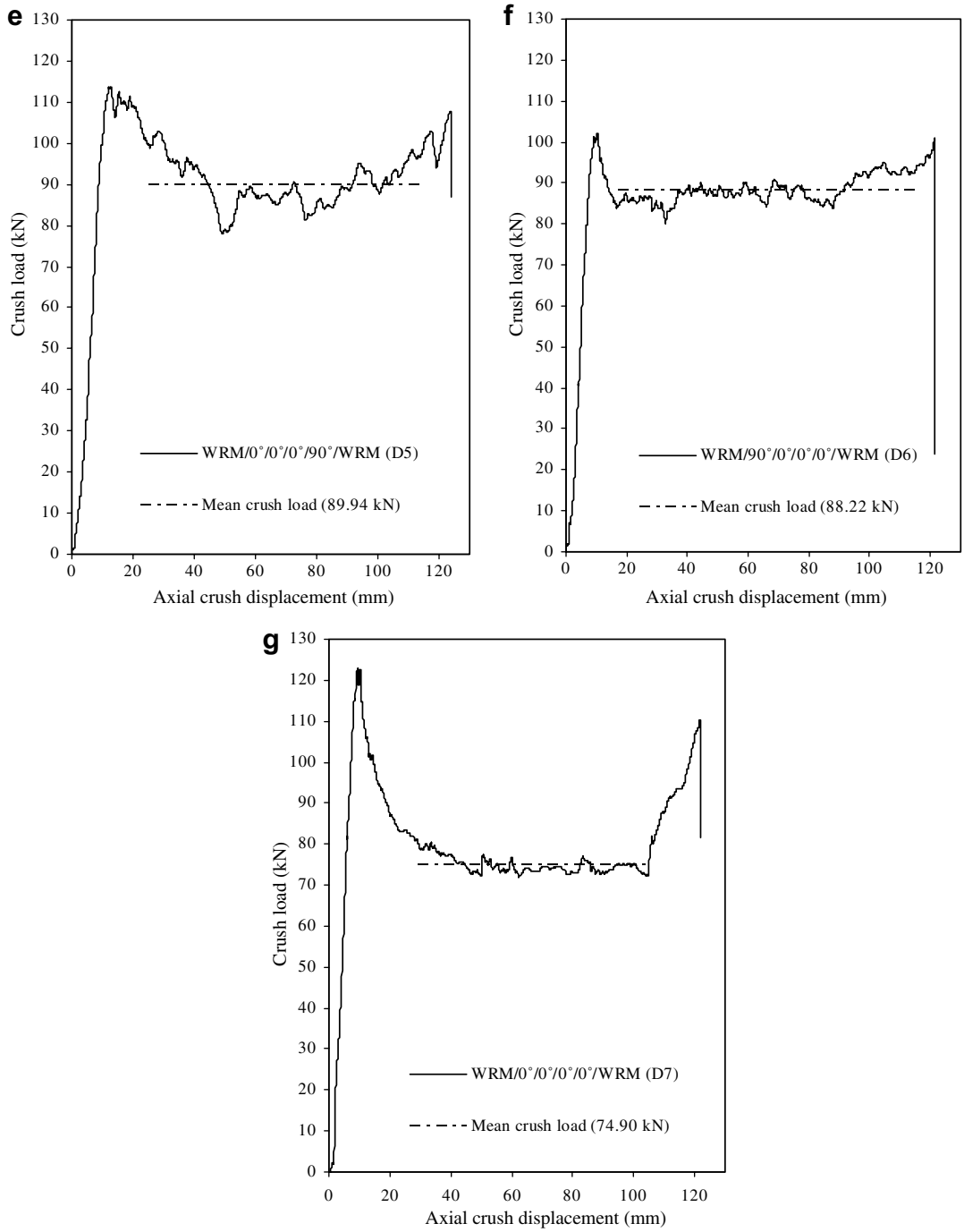

Fig. 7 (*continued*)

3.4.2. Six-ply tubes ($D/t = 15$)

The increased circumferential fibre content in the six-layered WRM/$(90)_4$/WRM (D1) tubes resists axial crack formation, and hence only one axial crack is formed, and the petals are not formed. The crushed fibres in the form of almost circular strips are collectively assembled near the crush zone, and are shown in Fig. 5. Continuous frond formation is not observed in this D1 specimen. Comparing to circumferential fibres, the

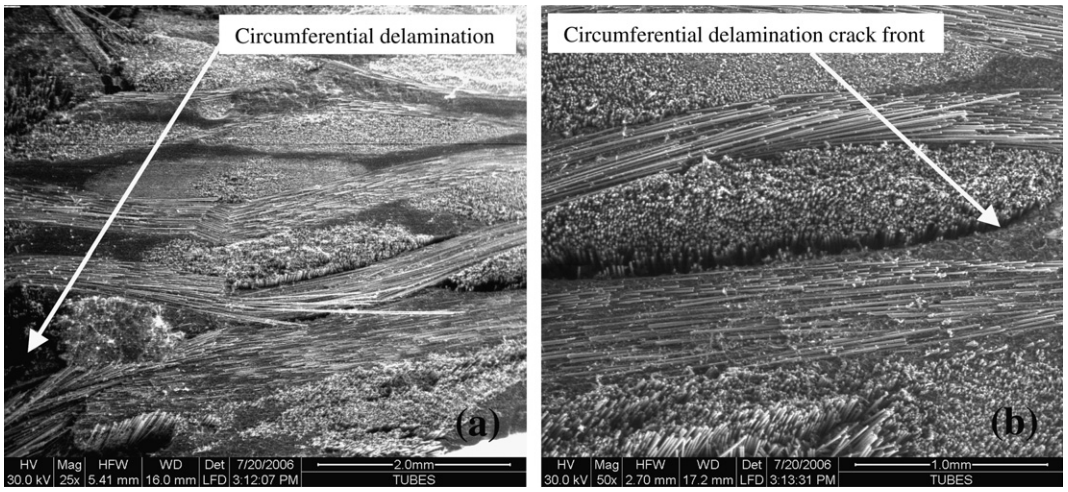

Fig. 8. SEM picture of crush zone in the cylindrical shell (a) delamination crack (b) crack front.

axial fibres offer very less resistance to axial crack formation and propagation, and hence the outer most axial fibres in the WRM/$(0)_2$/$(90)_2$/WRM (D2) specimens lead to the formation of eight petals. In case of WRM/$(90/0)_2$/WRM (D3) specimens, the outermost three layers flare outwards into fronds. But the axial cracks formed are not well defined as in case of C2, C4 and D7 specimens. In these D3 tubes, only five petals are formed and are shown in Fig. 5. The outermost circumferential fibres, offering high resistance to axial crack formation in the WRM/$(90)_2$/$(0)_2$/WRM (D4) specimens cause three petals almost in the form of bellows. Only five petals are formed due to resistance for axial cracking offered by 90° layer placed near the outer surface in the D6 tubes unlike in D5 tubes in which eight petals are formed. So, in the case of D7 specimens having higher proportion of axial fibres, the outermost WRM layer and its adjacent two axial layers flare outwards and cause well defined petal formation. The circumferential delamination is formed well in all the types of specimens except D1 specimen.

The D1 tubes have the lowest SEA, 31736 J/kg of all the D series tubes. When the proportion of 0° fibres is increased to 50%, the D2, D3 and D4 tubes have SEA, 14%, 36% and 49% higher than that of D1 tubes, respectively. The SEA of D5 and D6 tubes are 52% and 59% higher than that of D1 specimens, respectively. The D7 tubes have SEA, 43% higher than that of D1 tubes. Fig. 10 shows that the SEA rises with proportion of axial fibre content up to about 68% of 0° fibres, above which the crushing resistance decreases. It is observed during experiments that tubes undergo stable crushing when the axial cracks are initiated. The mild load oscillation is observed in WRM/$(0)_2$/WRM and WRM/$(0)_4$/WRM tubes, comparing to other tubes. In case of WRM/$(0)_2$/WRM, WRM/$(0)_2$/$(90)_2$/WRM and WRM/$(0)_4$/WRM tubes, stable crushing starts after around 30 mm compression, while the WRM/0/90/WRM and WRM/$(0)_3$/90/WRM tubes around 20 mm; a characteristic phenomenon which is not observed in other tubes.

3.5. Effect of stacking sequence upon specific energy

The SEA variation with the proportion of 0° fibres content (Figs. 9 and 10) shows that the SEA is influenced by the stacking sequence and the proportion of 0° and 90° fibres. The SEA increases with increase in proportion of 0° fibre content for the same thickness of tubes. It is also observed that for the same amount of 0° fibre content, the lay-up sequence influences the SEA. There is a constraint in bending radius of curvature for the material splaying inwards, which is not for the material splaying outwards. The maximum allowable radius of curvature for the material splaying inside is half of the inside tube diameter. The presence of axial fibres offers higher bending stiffness, and hence the axial layers placed near the inner surface of tube dissipates large amount of energy against bending inside the tube through constrained bending radius of curvature. The circumferential fibres placed close to the outer surface of the tube offer resistance to axial cracking,

Table 4
Specific energy absorption of cylindrical shells

Sl. No	Specimen ID	Lay-up sequence of layers	Axial (0°) fibre content (%)	Tube length (mm)	Inner dia, D (mm)	Thickness (mm)	Number of petals formed	Interlaminar fracture toughness G_{Ic} (kJ/m^2)	SEA (J/kg)			
		Outer Inner							Sample 1	Sample 2	Sample 3	Average ± Std dev
Four-layered tubes												
1	C1	WRM/$(90)_2$/WRM	22.4	156.5	63	2.5	2[a]	0.481 ± 0.015	35690	35250	35929	35623 ± 344
2	C2	WRM/0/90/WRM	50	153	63.4	2.9	7–8	0.524 ± 0.006	36948	36550	36203	36567 ± 372
3	C3	WRM/90/0/WRM	50	156.5	64	2.5	3	0.524 ± 0.006	39302	38530	38934	38922 ± 386
4	C4	WRM/$(0)_2$/WRM	77.6	158	63.4	2.9	8	0.358 ± 0.075	44868	44120	44591	44526 ± 378
Six-layered tubes												
5	D1	WRM/$(90)_4$/WRM	14.5	156	63.5	4.4	0[b]	0.481 ± 0.015	32850	31610	30748	31736 ± 1056
6	D2	WRM/$(0)_2$/$(90)_2$/WRM	50	156.5	64.25	4.1	8	0.524 ± 0.006	34415	36540	37923	36292 ± 1767
7	D3	WRM/(90/$0)_2$/WRM	50	156	63.5	4.4	5	0.524 ± 0.006	42705	42978	43434	43039 ± 368
8	D4	WRM/$(90)_2$/$(0)_2$/WRM	50	155	64.4	4.1	3[a]	0.524 ± 0.006	48560	47260	46083	47301 ± 1239
9	D5	WRM/$(0)_3$/90/WRM	67.8	155	63.5	4.8	8	0.358 ± 0.075	46765	48251	49521	48179 ± 1379
10	D6	WRM/90/$(0)_3$/WRM	67.8	156.5	63.5	4.2	5–6	0.358 ± 0.075	49935	50350	51140	50475 ± 612
11	D7	WRM/$(0)_4$/WRM	85.5	155	63.5	4.2	8	0.358 ± 0.075	45994	45261	44798	45351 ± 603

0°-fibre orientation along the tube axis; 90°-fibre orientation along the hoop direction.
[a] Material crushed in the form of Bellows.
[b] No petals. Almost circular strips are observed.

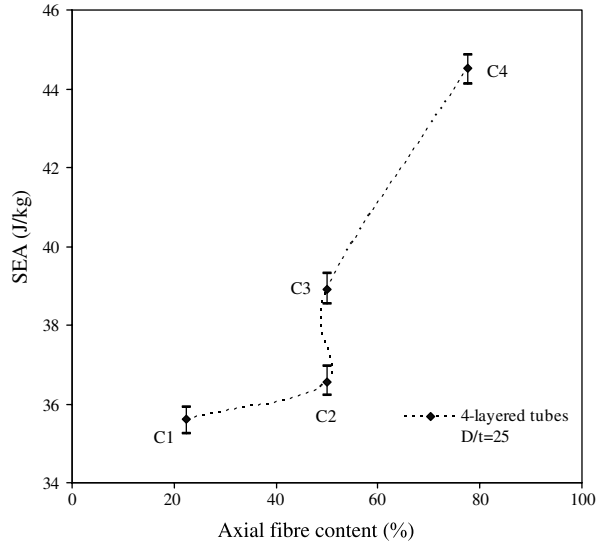

Fig. 9. SEA variation with proportion of axial fibre content ($D/t = 25$).

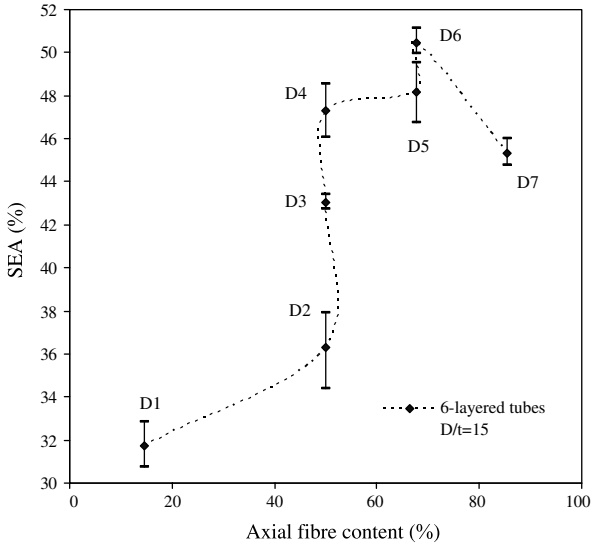

Fig. 10. SEA variation with proportion of axial fibre content ($D/t = 15$).

and leads to higher energy dissipation through petalling. Placement of 0° fibres close to the outer surface of the tube wall leads to more number of petal formation as in C2, C4, D2 and D7 specimens.

The C2 and C3 tubes have same proportion (50%) of fibres along axial and circumferential directions, but the WRM/90/0/WRM (C3) tubes have SEA 6.5% higher than that of WRM/0/90/WRM (C2) tubes. This is because of the higher bending resistance offered by the material flared inwards due to the constraint in bending radius of curvature, comparing to the material that flared outwards, and higher resistance to axial cracks offered by 90° fibres flaring outwards.

Among the D2, D3 and D4 tubes having same amount of axial and circumferential fibres, D4 tubes have improved SEA due its proper stacking sequence. It is observed from these three tubes that laying circumferential fibres close to the outer surface and axial fibres close to the inner surface improves the SEA. So, the D3 and D4 tubes have SEA 19% and 30% higher than that of D2 tubes, respectively.

Though both D1 and D4 tubes have same amount of circumferential fibres in the outer half of the tube thickness, D4 tubes are crushed into petals almost in the form of bellows, whereas the D1 tubes are crushed into almost circular strips. This is because, the mid-plane interface in the D1 tubes have circumferential fibres in the middle which are acting together as a single layer, and offer more resistance to axial cracking.

The resistance to axial crack offered by the 90° layer placed near the outer surface and the higher bending resistance offered by the 0° layers placed near the inner surface increases the SEA of D6 tubes, whereas in the D5 tube, the 90° layer placed near inner surface offers lesser bending resistance comparing to axial fibres, also less resistance to axial cracking offered by axial fibres placed near the outer surface comparing to 90° layers. Therefore, the D6 tubes have SEA, around 5% higher than that of D5 tubes, though both types of tubes have same proportion (68%) of axial fibres.

It is observed that SEA of six-ply tubes is higher than that of four-ply tubes. The WRM/90/0/WRM (C3) and WRM/$(90/0)_2$/WRM (D3) tubes have same content of circumferential fibres in the outer half of the tube wall thickness, but C3 tubes have three petals whereas D3 tubes have five petals. This is because, the content of circumferential fibres placed near the outer surface of the tube wall improves the energy absorption by offering resistance to axial crack, and depends on the tube thickness. This increases with increase in thickness, however, much amount of hoop fibres avoid the petalling event as in D1 tubes.

4. Analytical modeling

The composite tubular specimen shown in Fig. 3 is crushed axially, and the circumferential delamination takes place in the middle of the thickness. Delaminated layers are strained circumferentially and the cracks are formed in the axial direction. Due to these circumferential delamination and axial crack, petals are formed. The photographs of tested tubular specimens shown in Figs. 4 and 5 are the evidence for the above discussed mechanism. Crushing is progressed towards other end of tube through bending of petals away from the centre of the wall thickness, which are broken at the root of petal. Brittleness of composite tube material causes the crush zone to progress through successive cycles with stroke length, h. The idealized model of the crush zone is shown in Fig. 11.

The energy terms assumed to be involved in the crush zone of axially crushed tube are

(i) External work done by the crushing platen (W_e)
(ii) Energy dissipated during circumferential delamination (U_d)
(iii) Energy dissipated during petal formation (axial cracks) (U_a)

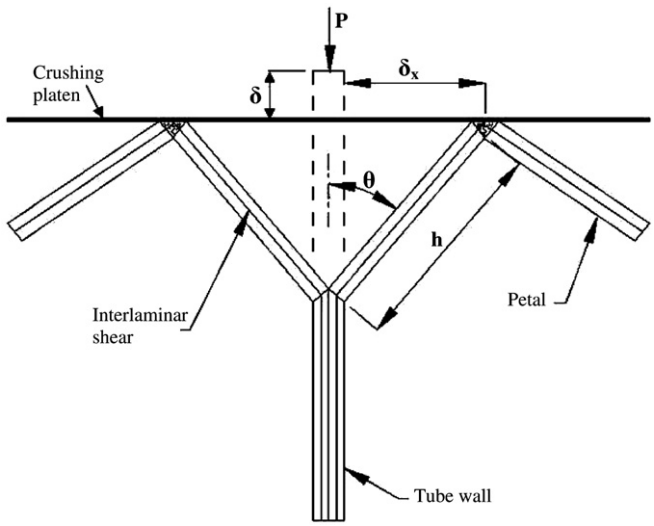

Fig. 11. Model of crush zone in the cylindrical tube wall.

(iv) Energy dissipated on bending of petals (U_b)
(v) Energy dissipated through interlaminar shear deformation in the petals during bending(U_s)
(vi) Energy dissipated due to friction between crushing platen and petals (U_f).

The mode I interlaminar fracture toughness, G_{Ic} and SEA are experimentally studied, and these values are used for energy calculations. The work done on the specimen is dissipated through the remaining five energy terms.

4.1. External work (W_e)

The work done by external load, P on the crushing displacement, δ is

$$W_e = P\delta \tag{2}$$
$$\delta = (h - h\cos\theta)$$

The maximum work done by the external force, when $\theta = 90°$, i.e., $\delta = h$, the crush length of single stroke is

$$W_e = Ph \tag{3}$$

4.2. Energy required for circumferential delamination (U_d)

The energy released through delamination to occur circumferentially in a single stroke is

$$U_d = G_{Ic}2\pi rh \tag{4}$$

where G_{Ic} is the critical strain energy release rate per unit interlaminar delaminated crack area and h is the crack length for single stroke. G_{Ic} is determined experimentally through DCB test as per ASTM D5528-01.

4.3. Energy required for petal formation (axial cracks) (U_a)

According to Griffith energy criterion for fracture state, crack growth can occur if the energy required to form the additional crack surfaces (G) can just be delivered by the system as a release of strain energy. The G_I for in-plane mode I failure resulting axial cracks is given by

$$G_I = \frac{K_I^2}{E} \tag{5}$$

where K_I is the mode I stress intensity factor. For the linear crack of any number of petals, K_I is approximated (Landkof and Goldsmith, 1985) as

$$K_I = \sigma\sqrt{\pi h}F(n) \tag{6}$$

$F(n)$ is a function of number of petals, n and σ is the circumferential stress. Hence Eq. (5) becomes

$$G_I = \frac{\pi h\sigma^2 F^2(n)}{E} \tag{7}$$

and

$$F(n) = \frac{2}{\sqrt{n}} \tag{8}$$

As discussed earlier the material splaying outwards flares into petals, and the material splaying inwards just bends without petalling. So, the total axial crack area is $A = 2(\frac{t}{2})hn$, where t is the thickness of tube wall. Therefore the total energy required for the formation of axial cracks is

$$U_a = \frac{\pi h\sigma^2}{E}\left(\frac{2}{\sqrt{n}}\right)^2 (thn) \tag{9}$$

The number of petals, n observed during experiments is reported in Table 4. Though the axial cracks are initiated by local buckling of the chamfered portion in the tube under axial compression, the axial cracks are propagated due to the tensile hoop stress in the progressive crush zone. Since this analytical model is focused on the steady state progressive crush zone, it is assumed that the failure stress due to the circumferential strain is equal to the ultimate fracture strength in uni-axial tension (σ_u). Therefore the tensile strength values of the planar specimens are used in the model for estimating the energy released through petal formation (axial cracking). The series of two and three-ply laminates provide strength values (Table 2) of material in the outer and inner half of the tube thickness, which are flaring outwards and inwards in the four and six-ply tubes, respectively. The corresponding strength values of outer and inner half of the tube thickness are substituted in the analytical expression. At fracture $\sigma = \sigma_u$, thus

$$U_a = \frac{4\sigma_u^2 \pi h^2 t}{E} \tag{10}$$

Also, the value of E is calculated from linear stress strain relation

$$E = \frac{\sigma_u}{\varepsilon} = \frac{\sigma_u r}{h \sin\theta} \tag{11}$$

Thus the total energy required for petal formation, U_a, is

$$U_a = \frac{4\sigma_u \pi h^3 t \sin\theta}{r} \tag{12}$$

4.4. Energy required for bending of petals (U_b)

Petals with length equal to axial crack length of single cycle, h are formed during axial crushing, and are assumed as cantilever beams of constant thickness and rectangular shape at each stage of crack propagation. The fixed portion of this beam is broken by bending at the end of every cycle, and the circumferential delamination followed by axial cracks propagates for next cycle. The fully plastic state bending moment per unit width $M_b = \frac{\sigma_y t_{petal}^2}{4}$ is used for calculating the petal bending work in case of metallic tubes, where σ_y is bending yield strength (Reddy and Reid, 1986). Here, the fracture state bending moment per unit width $M_b = \frac{\sigma_b t_{petal}^2}{4}$ is used for calculating petal bending work for thermoset glass/polyester composites, where σ_b is the flexural strength. Energy required for breaking the petals by bending both inside and outside of the wall is

$$U_b = \int_0^{\frac{\pi}{2}} \frac{\sigma_b b t^2 \, d\theta}{8} = \frac{\sigma_b b t^2 \pi}{16} \tag{13}$$

where b is the total width of petals ($b = 2\pi r$) and θ is the bending angle of petals. This energy is maximum when θ is equal to 90°.

4.5. Energy dissipated through interlaminar shear deformation in the petals during bending (U_s)

The energy dissipated by the shear deformation of the matrix material between layers due to bending of petals of length h (length of crush zone) is

$$dU_s = \int \sigma_s \varepsilon \, dV$$

$$\varepsilon = \frac{\delta_x}{h}$$

$$U_s = \int_0^{\frac{\pi}{2}} \sigma_s \left(\frac{h \sin\theta}{h}\right)(2\pi r t h) d\theta = \int_0^{\frac{\pi}{2}} 2\pi r t \sigma_s \sin\theta \, d\theta \tag{14}$$

where σ_s is the interlaminar short beam shear strength and $\delta_x = h\sin\theta$.

4.6. Energy dissipated due to friction between the crushing platen and petals (U_f)

The debris inside the circumferential delamination crack and petals are rubbing on the crushing platen during the progression of crush zone. The energy dissipated due to friction between the petals that flare both inside and outside the tube wall and the crushing platen (Tao et al., 1993) is

$$U_{\mathrm{f}} = 2\mu P\delta_x \tag{15}$$

where $\delta_x = h\sin\theta$. The co-efficient of friction between petal and crushing platen, μ is equal to approximately 0.35 (Gupta et al., 1997). The frictional energy dissipation reaches its maximum value, when $\theta = 90°$, i.e., $\delta_x = h$, and hence

$$U_{\mathrm{f}} = 2\mu Ph \tag{16}$$

According to the balance of energy, the work done on the specimen is equal to the sum of energy dissipated by the specimen

$$W_{\mathrm{e}} = U_{\mathrm{d}} + U_{\mathrm{a}} + U_{\mathrm{b}} + U_{\mathrm{s}} + U_{\mathrm{f}}$$

$$P(\delta - 2\mu\delta_x) = [G_{\mathrm{Ic}}2\pi rh] + \left[\frac{4\sigma_{\mathrm{u}}\pi h^3 t\sin\theta}{r}\right] + \left[\int_0^{\frac{\pi}{2}} \frac{\sigma_{\mathrm{b}} bt^2\,\mathrm{d}\theta}{8}\right] + \left[\int_0^{\frac{\pi}{2}} 2\pi rt\sigma_{\mathrm{s}}\sin\theta\,\mathrm{d}\theta\right]$$

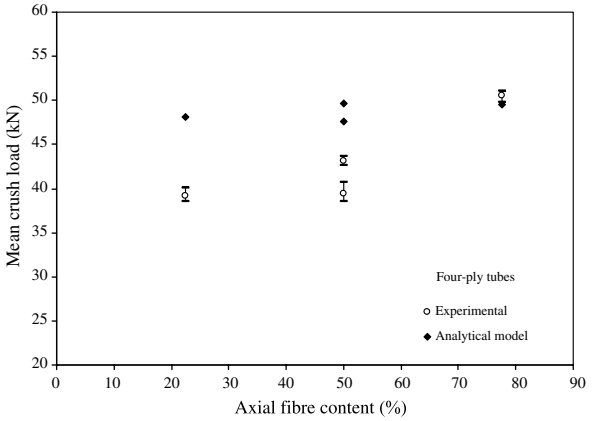

Fig. 12. Mean crush load of axially crushed cylindrical shells with various proportion of axial/circumferential fibre content ($D/t = 25$).

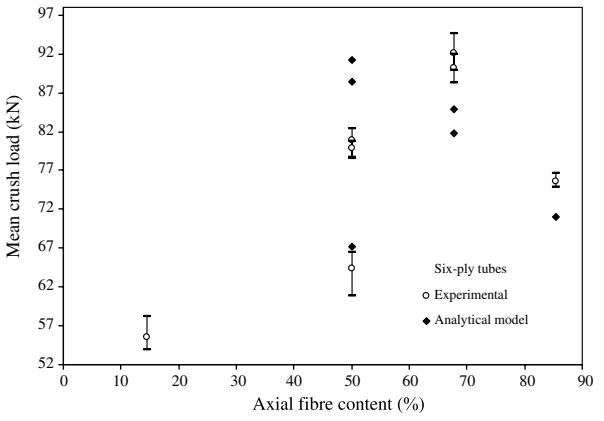

Fig. 13. Mean crush load of axially crushed cylindrical shells with various proportion of axial/circumferential fibre content ($D/t = 15$).

Table 5
Experiments and theoretical values of mean crush load

Sl. No.	Specimen ID	Specimen	Mean crush load (N)					Error (%) = (Exp − Theo) × 100/Exp
			Experimental				Theoretical	
			Sample 1	Sample 2	Sample 3	Average ± Std dev		
Four-layered tubes								
1	C1	WRM/$(90)_2$/WRM	40023	38955	38559	39179 ± 757	48080	22
2	C2	WRM/0/90/WRM	43589	42652	43256	43165 ± 474	47630	10
3	C3	WRM/90/0/WRM	40684	38900	38552	39378 ± 1143	49710	22
4	C4	WRM/$(0)_2$/WRM	51116	49795	50717	50542 ± 677	49500	2
Six-layered tubes								
5	D1	WRM/$(90)_4$/WRM	58213	53870	54599	55560 ± 2325	No progressive crushing and petal formation	
6	D2	WRM/$(0)_2$/$(90)_2$/WRM	60893	66437	65670	64333 ± 3000	67160	4
7	D3	WRM/$(90/0)_2$/WRM	80190	78644	80743	79859 ± 1087	88420	10
8	D4	WRM/$(90)_2$/$(0)_2$/WRM	82397	81797	78490	80894 ± 2100	94710	12
9	D5	WRM/$(0)_3$/90/WRM	89939	91833	94569	92113 ± 2320	81720	11
10	D6	WRM/90/$(0)_3$/WRM	88224	90245	91938	90135 ± 1850	84920	5
11	D7	WRM/$(0)_4$/WRM	76558	75118	74904	75526 ± 890	71010	5

The energy terms related to external work, frictional work, circumferential delamination work, interlaminar shear work and petal bending work are maximum when bending angle θ is equal to 90°. The thickness and diameter of cylindrical shell is constant throughout the length of specimen, and hence the crush load oscillates in a regular way in the stable controlled progressive crush zone, and the average load per wave is same throughout the stable crush length of specimen. So the integrated four terms are added.

$$P = \frac{1}{h(1-2\mu)}\left([G_{Ic}2\pi rh] + \left[\frac{4\sigma_u \pi h^3 t \sin\theta}{r}\right] + \left[\frac{\sigma_b b t^2 \pi}{16}\right] + [2\pi rt\sigma_s]\right) \tag{17}$$

The expression for θ in the energy term related to axial crack is obtained by equating circumferential strain to the fracture strain in uni-axial tension, $d\varepsilon$. Thus

$$\sin\theta = \frac{d\varepsilon\, r}{h}$$

Minimization of load P in Eq. (17), i.e., $\frac{\partial P}{\partial h} = 0$, leads to

$$h = \left(\frac{r^2 t\theta}{32\sin\theta}\right)^{1/3} \tag{18}$$

The mean crush load of cylindrical shells under axial compression are predetermined by incorporating the values of G_{Ic} from Table 3, σ_u, σ_b and σ_s from Table 2, and h obtained through iteration from Eq. (18) in the energy balance Eq. (17).

4.7. Validation of theoretical model

The mean crush load and SEA of composite cylindrical shells under axial compression are predetermined from the analytical model developed based on energy approach. Figs. 12 and 13 show the same trend of mean crush load obtained from experiments and analytical model for both four and six-layered specimens. The experimental results are used for validation of analytical model results. The deviational errors are reported in Table 5. The results from the analytical model show good agreement with experimental results. This model is valid only for tubes that undergo stable progressive crushing through the formation of petals during axial compression.

The D1 tubes are crushed in the unstable mode and do not undergo stable crushing mechanisms like circumferential delamination and axial cracking, and hence Table 5 shows higher deviational error between experimental and model results for D1 tubes. In the analytical modeling, the energy dissipation through petal formation (axial cracking) is considered only for the material splaying outwards into petals and not for the material splaying inwards. But in actual case, for the higher proportion of axial fibre content, the axial cracks are initiated without mere formation of petals in the material splaying inwards. This energy dissipation which is relatively small amount, is not considered in the modeling. Therefore the model underestimates the mean crush load for higher proportion of axial fibre content. It is observed from the Eq. (12) that energy dissipated through axial crack formation, U_a depends on the tensile hoop strength of layers placed in the outer half of the tube wall thickness, which are higher for circumferential fibres. Through proper stacking sequence the energy dissipated through axial crack propagation is improved from 31 to 185 J for single stroke length.

5. Conclusions

The trend of petalling event and the number of petals formed depend on the fibre orientation and stacking sequence of tubes. The presence of hoop fibres nearer to outer surface of the tube wall offers resistance to axial cracking and leads to higher energy dissipation through petalling, however much amount of hoop fibres avoids the petalling event. The content of circumferential fibres placed close to the outer surface of the tube wall that improves the energy absorption by offering resistance to axial crack, depends on the tube thickness, and it increases with increase in thickness. The axial fibres placed close to inner surface of tube wall offer considerable resistance to bending, due to constrained bending radius of curvature inside the tube, and lead to better energy absorption; while the axial fibres placed close to outer surface lead to more number of petal

formation, a stable crushing mechanism. Thus in the tubes undergo petalling, presence of axial fibres close to inner surface, and the proper proportion of circumferential fibres close to outer surface of the tube wall lead to higher energy dissipation. The energy dissipation in the form of circumferential delamination increases for higher values of mode I strain energy release rate, G_{Ic}. Results obtained from the analytical model show good agreement with experimental results. Higher proportion of fibres oriented along the length of the planar specimens improves the basic mechanical properties like tensile, flexural and interlaminar short beam shear strengths.

References

Alexander, J.M., 1960. An approximate analysis of the collapse of thin cylindrical shells under axial loading. Quarterly Journal of Mechanics and Applied Mathematics XIII (Pt. 1), 10–15.

ASTM Designation: D5528-01, 2000. Standard test method for Mode I interlaminar fracture toughness of unidirectional fiber-reinforced polymer matrix composites. Annual Book of ASTM Standards 2000, vol. 15.03. ASTM, Philadelphia.

Atkins, A.G., 1987. On the number of cracks in the axial splitting of ductile metal tubes. International Journal of Mechanical Sciences 29 (2), 115–121.

Atkins, A.G., Afzal khan, M., Liu, J.H., 1998. Necking and radial cracking around perforations in thin sheets at normal incidence. International Journal of Impact Engineering 21 (7), 521–539.

Bisagni, C., Di Pietro, G., Fraschini, L., Terletti, D., 2005. Progressive crushing of fibre-reinforced composite structural components of a Formula One racing car. Composite Structures 68 (4), 491–503.

Daniel, L., Hogg, P.J., Curtis, P.T., 2000. The crush behavior of carbon fibre angle-ply reinforcement and the effect of interlaminar shear strength on energy absorption capability. Composites Part B: Engineering 31 (5), 435–440.

Farley, G.L., 1991. The effects of crushing speed on the energy absorption capability of composite tubes. Journal of Composite Materials 25, 1314–1329.

Farley, G.L., Jones, R.M., 1992. Prediction of energy absorption capability of composite tubes. Journal of Composite Materials 26 (3), 388–404.

Gupta, N.K., Abbas, H., 2000. Mathematical modeling of axial crushing of cylindrical tubes. Thin Walled Structures 38, 355–375.

Gupta, N.K., Velmurugan, R., Gupta, S.K., 1997. An analysis of axial crushing of composite tubes. Journal of Composite Materials 31 (13), 1262–1286.

Hamada, H., Ramakrishna, S., 1995. Scaling effects in the energy absorption of carbon-fibre/PEEK composite tubes. Composites Science and Technology 55 (3), 211–221.

Hosseinzadeh, R., Shokrieh, Mahmood M., Lessard, Larry B., 2005. Parametric study of automotive composite bumper beams subjected to low-velocity impacts. Composite Structures 68 (4), 419–427.

Hull, D., 1991. A unified approach to progressive crushing of fibre-reinforced composite tubes. Composite Science Technology 40, 377–421.

Landkof, B., Goldsmith, W., 1985. Petalling of thin, metallic plates during penetration by cylindro-conical projectiles. International Journal of Solids Structures 21 (3), 245–266.

Mamalis, A.G., Robinson, M., Manolakos, D.E., Demosthenous, G.A., Ioannidis, M.B., Carruthers, J., 1997. Crashworthy capability of composite material structures. Composite Structures 37 (2), 109–134.

Mamalis, A.G., Manolakos, D.E., Ioannidis, M.B., Papapostolou, D.P., 2004. Crashworthy characteristics of axially statically compressed thin-walled square CFRP composite tubes: experimental. Composite Structures 63 (3-4), 347–360.

Mamalis, A.G., Manolakos, D.E., Ioannidis, M.B., Papapostolou, D.P., 2006. The static and dynamic axial collapse of CFRP square tubes: finite element modeling. Composite Structures 74 (2), 213–225.

Quek, S.C., Waas, Anthony M., Hoffman, Jennifer, Agaram, Venkatesh, 2001. The crushing response of braided and CSM glass reinforced composite tubes. Composite Structures 52 (1), 103–112.

Reddy, T.Y., Reid, S.R., 1986. Axial splitting of circular metal tubes. International Journal of Mechanical Sciences 28 (2), 111–131.

Reddy, T.Y., Wall, R.J., 1988. Axial compression of foam-filled thin-walled circular tubes. International Journal of Impact Engineering 7 (2), 151–166.

Shah Khan, M.Z., Mouritz, A.P., 1996. Fatigue behavior of stitched GRP laminates. Composites Science and Technology 56 (6), 695–701.

Solaimurugan, S., Velmurugan, R., 2007. Progressive crushing of stitched glass/polyester composite cylindrical shells. Composites Science and Technology 67 (3–4), 422–437.

Tao, W.H., Robertson, R.E., Thornton, P.H., 1993. Effects of material properties and crush conditions on the crush energy absorption of fiber composite rods. Composites Science and Technology 47 (4), 405–418.

Tao, Z., Dai-ning, F., Tian-jian, L., 2005. Dynamic crashing and impact energy absorption of 3D braided composite tubes. Materials Letters 59, 1491–1496.

Velmurugan, R., Solaimurugan, S., 2007. Improvements in Mode I interlaminar fracture toughness and in-plane mechanical properties of stitched glass/polyester composites. Composites Science and Technology 67 (1), 61–69.

Velmurugan, R., Gupta, N.K., Solaimurugan, S., Elayaperumal, A., 2004. The effect of stitching on FRP cylindrical shells under axial compression. International Journal of Impact Engineering 30 (8–9), 923–938.

Wierzbicki, T., 1999. Petalling of plates under explosive and impact loading. International Journal of Impact Engineering 22 (9–10), 935–954.